

# Chapter 1

## Introduction

The phenomenon of (passive) Brownian Motion is a well investigated topic in physics since 1827, when Robert Brown studied pollen grains suspended in water, finding out that they moved in an erratic, extremely irregular way. After experimenting with non-organic suspended particles, he concluded that this random motion must be caused by the fluid. Physically, it is possible to define Brownian motion as the effect of the impacts between the fluid particles and the suspended grain: since fluid's motion can be described by thermodynamics at particle level as a series of random fluctuations, impacts will be random as well, leading to an intrinsic stochasticity in the position of the particle. A notable contribution in the mathematical formalization of Brownian motion, based on random impacts, was made by Einstein and Langevin **gardiner\_handbook\_2004**. Later, Ornstein and Uhlenbeck **uhlenbeck\_theory\_1930** studied some fundamental properties such as the mean-square displacement of a Brownian particle in 2D. Although relatively simple, this model is able to explain the statistical properties of particles suspended in a medium, but more can be added to it to mimic real world behaviors. There are some kind of *particles*, such as bacteria, algae or other living beings that are able to propel themselves with a deterministic velocity, leading to more complex behaviors than the ones observed with pollen grains in water. One of the models that can be created adding deterministic properties along the stochastic behavior of a Brownian motion is Active Brownian Particles (ABPs).

Active particles are distinguished by their ability to extract energy from the environment and use it to autonomously propel themselves, thus making them a fundamental model for non-equilibrium active matter systems. The motility mechanism can be mechanic, like cilia or flagella used by micro-organisms, or thermo- and chemodynamic, like phoresis of various nature **moran\_phoretic\_2017**.

Incorporating self-propulsion within the Brownian framework enables the emergence of numerous novel behaviors, among which self-organization being noteworthy and the subject of this thesis. Across different systems, details about a single particle may differ, especially in propulsion mechanisms, nonetheless it is possible to build minimal statistical physics models that mimic real world dynamics, leading the way to the discovery of new physics as well as methods to analyze real living beings' behaviors and new ideas in material science.

## 1.1 Microrobotics and CELLOIDS

The first one to bring the concept of robotics at micro scale, especially for medical applications into a scientific context was Richard Feynman in the famous 1959 CalTech conference **Feynman Feynman**, from which the following quote is taken:

*Many of the cells are very tiny, but they are very active [...] Consider the possibility that we too can make a thing very small which does what we want — that we can manufacture an object that maneuvers at that level!*

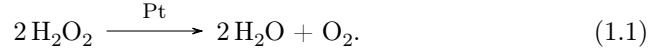
*[...] it would be interesting in surgery if you could swallow the surgeon. You put the mechanical surgeon inside the blood vessel and it goes into the heart and "looks" around. [...] It finds out which valve is the faulty one and takes a little knife and slices it out. Other small machines might be permanently incorporated in the body to assist some inadequately functioning organ.*

The scaling laws of physical quantities, especially regarding friction and hydrodynamics, makes it challenging to construct a micrometer scale robot which is just a miniaturized version of a macroscopic one. Moving in a fluid for the  $\mu\text{m}$  size and speed of few  $\mu\text{m s}^{-1}$  we are interested in — meaning, at low Reynolds number ( $\text{Re} \equiv \rho v L / \eta$ ) — requires quite a different approach than what we are used to in the macroscopic world. When inertia is negligible, it is impossible to swim using a *reciprocal motion*, that is, a cyclic motion that follows the same path forward and back **purcell\_life\_1977**. Needless to say that turning a propeller with a miniaturized macroscopic motor won't be optimal at this scale, since its starting torque would be extremely large. These huge difficulties are encountered if one just wants to swim in a simple fluid. Using a micro robot inside a human body brings some other challenges in the problem, such as swimming in viscoelastic media like hyaluronic acid lattices or shrinking through the small interstices in between living cells. Most of the problems we enumerated have been solved by nature already e.g. immune cells can overcome pretty much all challenges mentioned in this paragraph. When trying to tackle said challenges a convenient approach would be imitating what has been already done in billions of years of evolution, instead of developing new strategies from scratch. When talking about microrobots, we need to be clear about what a microrobot *is*. A *robot* is “a machine that can perform a complicated series of tasks by itself” **robot\_def\_oxf**; a microrobot is defined as a robot with

- $\mu\text{m}$  -  $\text{mm}$  size
- some mobility properties
- no tether

and its design needs some key ingredients, such as an actuation to make it motile, control and a power source to be able to perform desired tasks, and capability to sense and perceive its environment **palagi\_bioinspired\_2018**. The aim of CELLOIDS, the project inside of which this work has taken place, is to build a micro-scale intelligent robotic system that takes inspiration from the amoeboid propulsion of immune cells. CELLOIDS' concept for a microrobot is using a

phospholipids GUV (Giant Unilamellar Vesicle), filled with ABPs, as robot's body. GUV's walls are deformable and can be pushed from the inside by ABPs, leading to further deformation and, in the end, motility, mimicking the behavior of living cells that can shrink through a biological tissue. A single ABP moves exploiting a mechanism called *self-phoresis*: phoresis is defined in fluid dynamics as the migration of a particle due to a gradient in a scalar quantity ( $\phi$ ) e.g. temperature or concentration. When the gradient is caused by the particle itself *self-phoretic* movement takes place. When studying motion of a particle in a fluid it is common to take as boundary condition a no-slip condition, i.e. the layer of fluid in contact with particle's solid boundary has zero velocity w.r.t. the boundary itself, while in the study of phoresis, a small interfacial layer around particle's surface shows, on macroscopic length scales, an apparent finite slip velocity. Slip velocity is proportional to the local gradient of  $\phi$  and the net migration of the particle is equal in magnitude and opposite in sign to the area average of the slip velocity on particle surface. When  $\phi$  is the concentration of some solute in the fluid, *diffusiophoresis* takes place; CELLOIDS tries to achieve this using active Janus particles, with an inert hemisphere and a catalytic one, which turns a fuel into some products generating a gradient in the concentration field in its vicinity; this makes the solvent flow around the particle causing it to move. One of the most studied Janus microparticle is  $\text{SiO}_2\text{-Pt}$ , where Pt is deposited on one hemisphere of the particle using a sputtering machine; the fuel is  $\text{H}_2\text{O}_2$  that is decomposed in



## 1.2 Objectives

In the previously described framework, collective behaviors and emergent properties of active particles populations, both self-induced and caused by the interaction with a rigid or deformable confinement, are of paramount importance for the microrobot to work properly.

The objective of this work is to develop a model, a simulation framework and a suite of analysis tools to study how an explicit interaction potential changes single and collective behaviors of an active particles system, while keeping in mind the experimental and applied point of view.

### 1.2.1 Objective 1: Minimal model accounting for aligning and non-aligning interactions

Active matter models can be either *dry* or *wet*: in *dry* models the solvent is not explicitly simulated while *wet* simulations solve equations both for colloidal and fluid particles, including all possible hydrodynamics. However, details about the hydrodynamic and electro-chemical fields around active particles are still a matter of investigation. Moreover, even if known, they can be realistically simulated only for individual or few particles. In terms of interactions among particles, two main types are reported in the literature: aligning interaction, involving the direction of particles, and non-aligning, which are independent on particles' direction of motion [callegari\\_numerical\\_2019](#).

This work aims at a minimal *dry* model that takes into account both aligning and non-aligning interactions in the attempt of matching experimental observations. Here, the term *minimal* means not only that a unique interaction potentials is used to couple both positional and orientational degrees of freedom, but also that this simple model could be enough to simulate real world phenomena without making assumptions on the hydrodynamics and chemistry involved.

Given this novel modeling technique and its implementation, the next step of this work is to obtain a qualitative, eyesight agreement between simulations and experiments, making the *in silico* experiment able to capture all the features and dynamics observed *in vitro* scanning the different parameters.

Moreover, with the right parameters, this model is capable of showing rich collective behaviors, making it a feasible alternative to study phase transitions in a statistical physics fashion. A well-known model in this field involving aligning interactions is the Vicsek model **vicsek\_novel\_1995**, which captures a plethora of natural world phenomena. Present work shows how a system with coupled positions and orientations can turn into a continuous Vicsek-like case study.

### 1.2.2 Objective 2: Analysis

Although qualitative agreement between experiments and simulations plays a significant role, we believe that developing quantitative tools to analyze structure and dynamics of the system we are studying is necessary to understand the ongoing physics. Moreover, with slight adjustments, these tools could easily be adapted to the analysis of experimental data, namely, positions of particles obtained from videos tracking.

Here, we used well-known analysis tools, as well as some novel instruments developed during this thesis work.

### 1.2.3 Objective 3: Inference and Deep Learning

The last objective of this thesis is to build a Deep Learning based tool which, when trained starting from a minimal set of simulation data, is able to infer the interaction potential between couples of particles both in simulated and experimentally observed situations.

## 1.3 State of the Art

*Active Matter* is a term that refers to systems, both at macroscopic and microscopic scales, which can be described as sets of individual constituents, often called active or self-propelled particles, that have the ability of taking energy from the environment or an internal source to convert it to work. Such systems show peculiar behaviors, both individual and collective, due to their intrinsic far-from-equilibrium physical properties, as well as interactions that may occur between active particles **menon\_active\_2010**, **ramaswamy\_active\_2017**.

In the next few sections, we will focus on how researchers have dealt with active matter systems, both from an individual behaviors and collective characteristics standpoint.

### 1.3.1 Interactions and emerging behaviours

Investigation of interactions and emerging behaviours (e.g. collective motion) is an extremely important topic in the field of active particles, since it not only lead to a better understanding of the physics behind active particle systems, but it helped developing physical and mathematical tools, such as order parameters, which can be used both in simulation and experimental context.

In the following section the Vicsek model will often be cited. This is the right time to give a brief introduction to it with the authors' words:

*The only rule of the model is: at each time step a given particle driven with a constant absolute velocity assumes the average direction of motion of the particles in its neighborhood of radius  $r$  with some random perturbation added.***vicsek\_novel\_1995**

Although extremely simple, this model is of paramount importance in the study of active matter since it can be studied in terms of a phase transition and recreates to some extent the behavior of real living systems.

Although not strictly related to the present work, **cavagna\_empirical\_2010**, **ballerini\_interaction\_2008** are essential papers for the study of collective motion. In these works, the problem of relating theoretical models and reality is tackled analyzing videos of starling swarms in order to understand characteristics of interactions. Understandably, the system studied by **cavagna\_empirical\_2010**, **ballerini\_interaction\_2008** is pretty different from the active Brownian particles ensemble investigated in this project, with the first difference being the dimensionality (a bird swarm, just like a school of fish moves in a 3D environment), but some of the problems reported in that paper are still present in these days active matter community.

As for the case of self-propelled particles, **martin-gomez\_collective\_2018** analyzes how an explicit polar aligning interaction can make the system transition to an ordered flocking phase, where almost all particles align their orientation in the same direction, even though an orientational noise is present. The model is built implementing an aligning torque between particles  $i$  and  $j$  which goes as  $K \sin(\theta_i - \theta_j)$ , only within a certain distance, and a repulsive potential  $\epsilon \left(\frac{\sigma}{r}\right)^{12}$  to take into account the excluded volume.

The parameters of the system are the Péclet number  $Pe = \frac{v_0}{\sigma\gamma}$  which is the ratio between the self propulsion velocity and the product of the characteristic length of the particles and the rotational diffusion coefficient, quantifying the relative importance of advection to diffusion in solute transport, and  $g = \frac{K}{4\pi\sigma^2\gamma}$  which quantifies the relative intensity of the orientational coupling strength and the reorienting noise. The order parameter is the mean global polarization

$$P = \frac{1}{N} \left| \sum_{k=1}^N \exp(i\theta_k(t)) \right| \quad (1.2)$$

which is  $\sim 0$  in the disordered phase and  $> 0$  in the flocking phase. The authors build a phase diagram in the  $Pe - g$  plane Figure 1.1, which shows the separation between disorder and flocking as well as intermediate clustering phases, one with a microscopic cluster structure and one where a macroscopic single cluster structure arises.

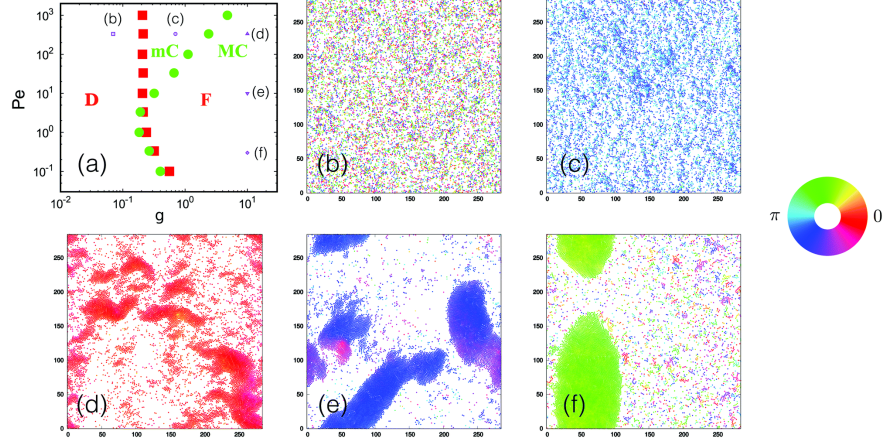


Figure 1.1: (a) Phase diagram in the  $g - Pe$  plane. (b-f) representing snapshots for different values of parameters. Adapted from [martin-gomez\\_collective\\_2018](#)

After noting that the phase transition happens with increasing  $g$  for any  $Pe > 1$ , authors focus on studying this transition in  $g$ , in the spirit of an equilibrium phase transition, with  $P$  as the order parameter and its susceptibility  $\chi = N(\langle P^2 \rangle - \langle P \rangle^2)$ . The behavior of the two quantities is similar to what is expected in a continuous phase transition with the critical coupling  $g^c = 0.21 \pm 0.02$  (Figure 1.3(a)).

The authors then focus on clustering phenomena, noting that the cluster size distribution decays exponentially for  $g < g^*$  and algebraically for  $g > g^*$ . This defines the two phases of microscopic and macroscopic clustering. Introducing two new order parameters

$$P_x = \left\langle \left| \frac{1}{N} \sum_{i=1}^N \cos(\theta_i) \right| \right\rangle; \quad P_y = \left\langle \left| \frac{1}{N} \sum_{i=1}^N \sin(\theta_i) \right| \right\rangle, \quad (1.3)$$

it is possible to distinguish between lane-like and band-like behavior in aligned clusters (Figure 1.2).

The authors use the radial distribution function

$$g(r) = \frac{1}{N} \left\langle \sum_{j \neq i} \sum_i \delta(r - |\mathbf{r}_i - \mathbf{r}_j|) \right\rangle \quad (1.4)$$

to characterize the global structure of the largest cluster. Increasing the coupling  $g$  at fixed Péclet number makes the peaks higher and shifts them to larger distances, showing that the system is developing a longer range order.

In [caprini\\_spontaneous\\_2020](#), authors investigate the alignment of instantaneous velocities in cases where motility-induced phase separation (MIPS) occurs. Most literature focuses on the effect that a central 2-body potential, or an explicit aligning interaction which couples the orientational degrees of freedom of single particles, has on the system, but the interplay between phase separation of particles systems and alignment in their velocity has hardly been studied.

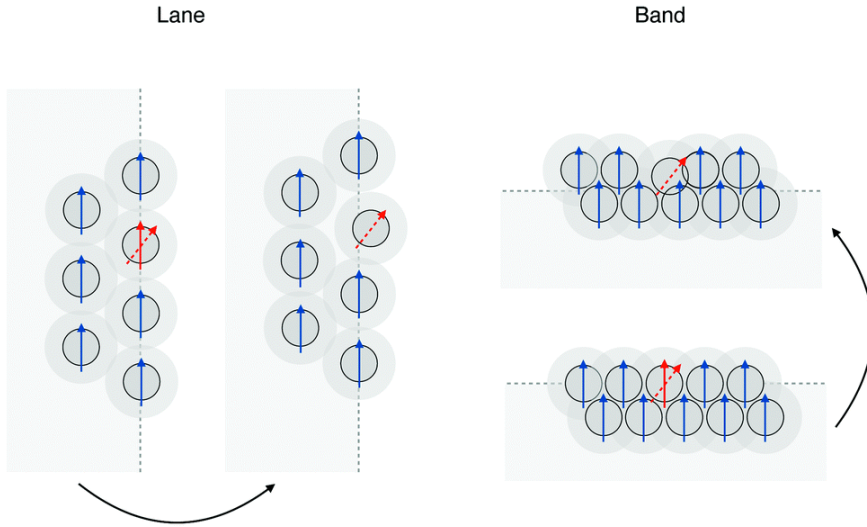
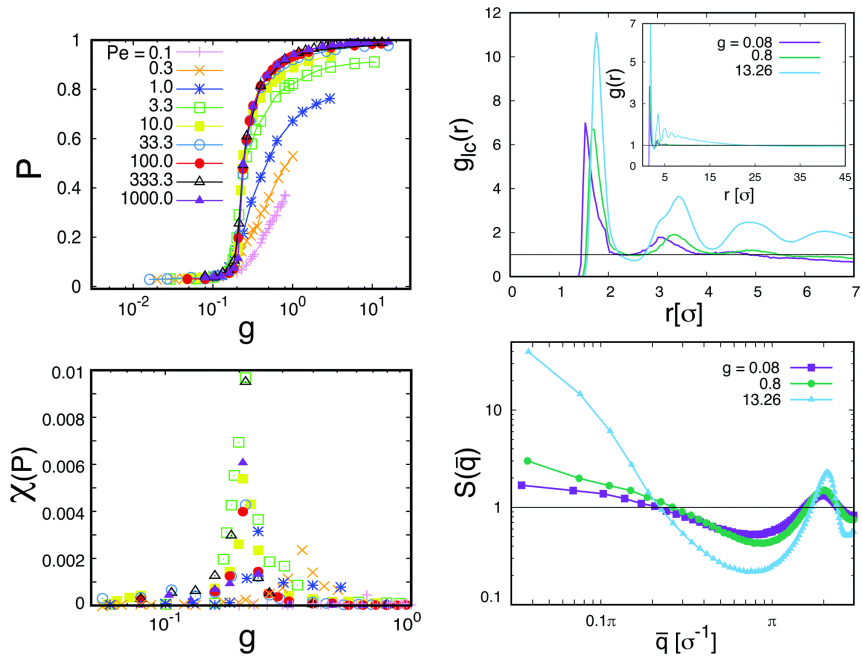


Figure 1.2: Different types of polarization. Adapted from martin-gomez\_collective\_2018.



(a) Phase transition behavior of polarization and its susceptibility

(b) Pair correlation function and static structure factor

Figure 1.3: Adapted from martin-gomez\_collective\_2018.

In the aforementioned paper, it is shown how, when active particle systems with a simple repulsive only Weeks-Chandler-Andersen potential phase-separate in a cluster, their velocity tend to form aligned domains, regardless the self propulsion orientation. For this reason, the global polarization is not a good order parameter, even when the computation is restricted to clusters, thus the authors introduce the spatial correlation function of the velocity orientation  $Q_i(r) = 1 - 2 \sum_j \frac{d_{ij}}{N_k \pi}$ , being  $d_{ij} = \min[|\theta_i - \theta_j|, 2\pi - |\theta_i - \theta_j|]$  the angular distance between two particles and  $N_k$  the number of particles in a circular shell around the  $i$ -th particle, taken with a thickness  $\bar{r} = \text{argmax}\{g(r)\}$ , and mean radius  $k\bar{r}$  with integer  $k$ .

It is possible to derive an order parameter from  $Q(R)$  integrating it

$$R = \int Q(r) dr \quad (1.5)$$

where the integral is performed on the cluster domain when present. This seems to be a good order parameter, since it makes it possible to distinguish the different phases of the system: varying the reorientation time  $1/D_r$ ,  $R$  is discontinuous at the point where the MIPS occurs and the result is consistent with established MIPS order parameters as shown in Figure 1.4.

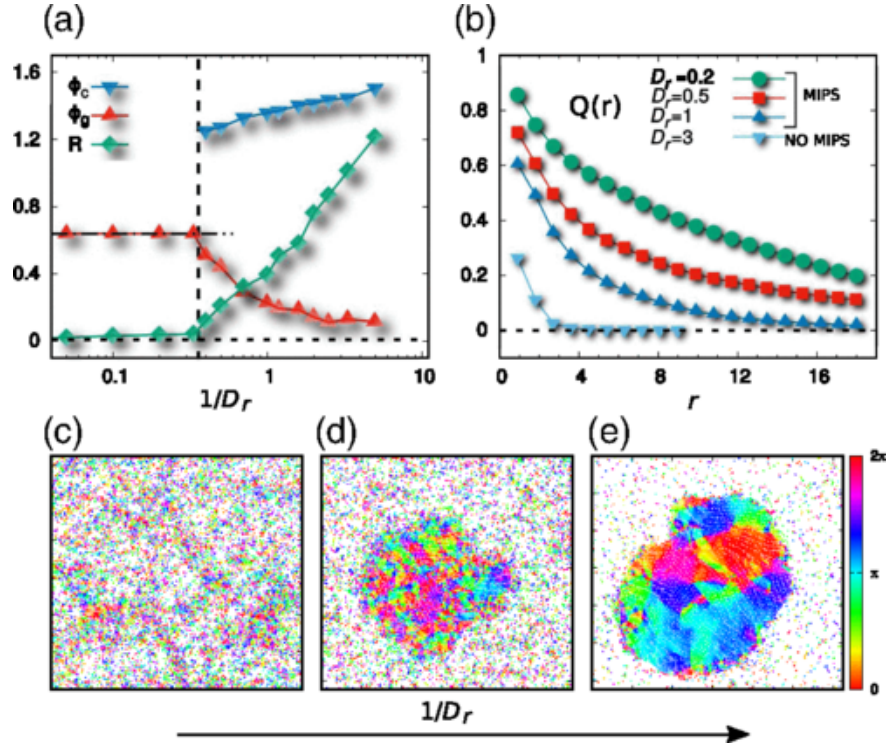


Figure 1.4: (a) Density as a function of  $1/D_r$  for gaseous and cluster phase. (b) Velocity alignment order parameter  $R$  as a function of  $1/D_r$ . (c-e) Representative snapshots for different values of  $D_r$ . Adapted from `caprini_spontaneous_2020`.

Furthermore, authors derive equation of motion for velocity, considering



hexagonal lattice arrangement of particles. Such equation involves a term which depends on the difference between particle's velocity and average velocity of the six surrounding it, thus re-obtaining a Vicsek-like model without a specific aligning interaction.

It is intuitive to think that a good animal collective motion model will have a vision. In ref. **negi\_emergent\_2022** authors implemented this vision with an aligning interaction similar to ref. **martin-gomez\_collective\_2018**. However, in the two models total torque is calculated differently; in ref. **negi\_emergent\_2022** the total torque on particle  $i$  is calculated taking into account only particles in the *vision cone* of particle  $i$ , i.e. a circular sector with center of mass of  $i$  as center as shown in Figure 1.5, with a given aperture angle and radius. This is useful to see what happens when *nonreciprocal* interactions, i.e. particle  $i$  feels the effect of particle  $j$  but the vice versa is not true.

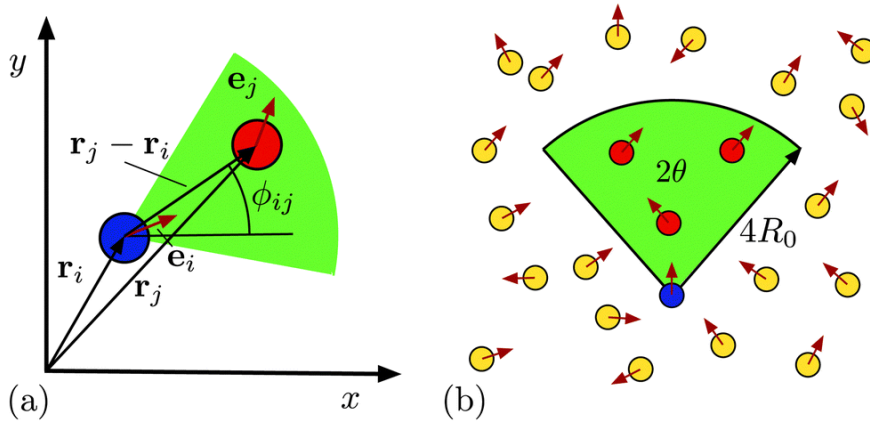


Figure 1.5: Schematic of nonreciprocal interaction with vision cone. Adapted from **negi\_emergent\_2022**.

The authors use tools, such as cluster size distribution, Mean Square Displacement (MSD) and velocity correlation function, to study the properties of a collection of *intelligent* active particles, but they also display some snapshot of the particles' simulation, which are particularly interesting to see what *can* happen when an interaction is acting on the system, both at small and large packing fraction.

### 1.3.2 Experimental analysis of collective behaviors

The interaction between active particles and their emergent collective behaviours have been studied also in experiments **singh\_pair\_2024**. When two  $\text{SiO}_2$ -Pt Janus particles come together in different configurations; authors model a collision analyzing the overlap between concentration fields around the two particles as well as the torque caused by the interaction between solvent flows around each hemisphere of a pair of Janus microswimmers. Although here we are trying to build a dry active matter simulation — means, absence of hydrodynamic and medium behavior is not simulated — papers like this accurately describe the phenomenology of these close encounters, which is essential to build minimal models that mimic real-world behavior. The main fact, supported both by

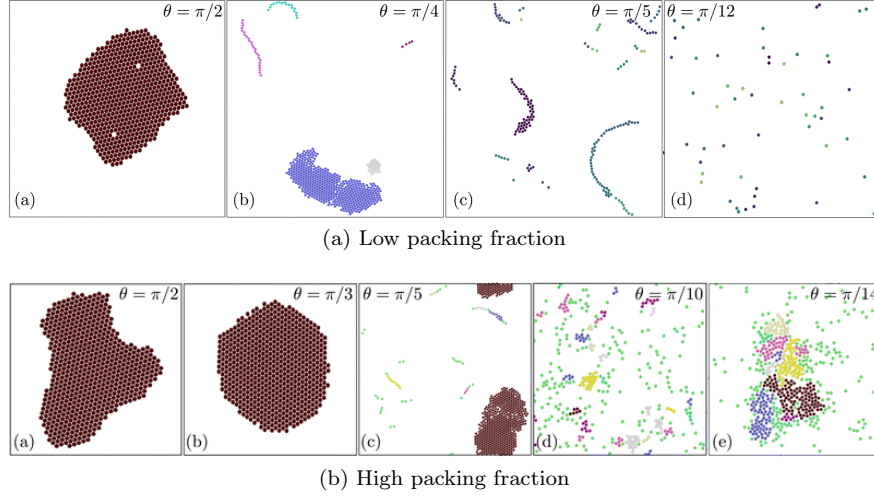


Figure 1.6: Representative snapshots for the configurations that model in **negi\_emergent\_2022** can achieve.

simulations and experimental evidence, to take away is that chemical and hydrodynamic interactions do not cause reorientation for pairs of particles separated by a long distance, and that leading effects are short-range chemical torques.

Dispersing Janus colloids in a  $\text{H}_2\text{O}_2$  solution in a quasi-2D environment, the types of configurations particles can scatter in are limited and categorized by **singh\_pair\_2024** in four dynamical states. The classification of both approach and departure states, along with a relative frequency histogram is in 1.7.

It is evident from this article that such particles exert a torque on each other at short range and this interaction, which is a product of the intrinsic asymmetry of a Janus colloid, must be considered in order to capture all the dynamics of these micro-swimmers.

Ref. **maity\_spontaneous\_2023** investigate what happens with a binary population of active colloidal particles, that is obtained by mixing particles of  $7\mu\text{m}$  and  $10\mu\text{m}$  in diameter. These colloids move due to a different mechanism than the one seen before, whose details will not be discussed here, called Quincke instability; with enough particle density, the solvent mediates an aligning interaction which makes the system undergo a Vicsek-like flocking transition that, within a circular confinement, takes place as a vortex motion. The two populations are distinguished by a difference in diameter and in velocity. Within some minutes, the initially uniform sample demixes spontaneously, heading to a segregated state where the two populations are well separated and their relative densities have a different radial profile, as shown in Figure 1.8.

**ostapenko\_curvature-guided\_2018**, in **ostapenko\_curvature-guided\_2018** look into the dynamics of biological micro-swimmers in a confinement. Authors tracked the movements of a single *Chlamydomonas reinhardtii* algae cell within a round and elliptical space. At the same time, they performed a simulation of the algae behavior as an ABP; to better model the dynamics, the alga's placeholder was a dumbbell shaped particle made of two attached spheres of

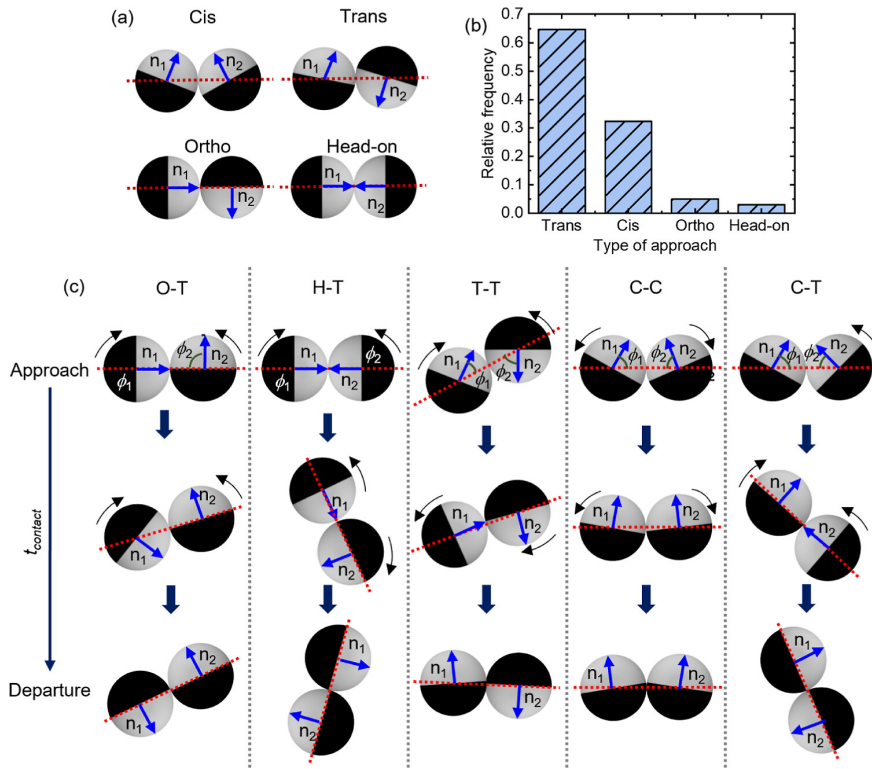


Figure 1.7: Classification of approach and departure configuration. Adapted from `singh_pair_2024`.

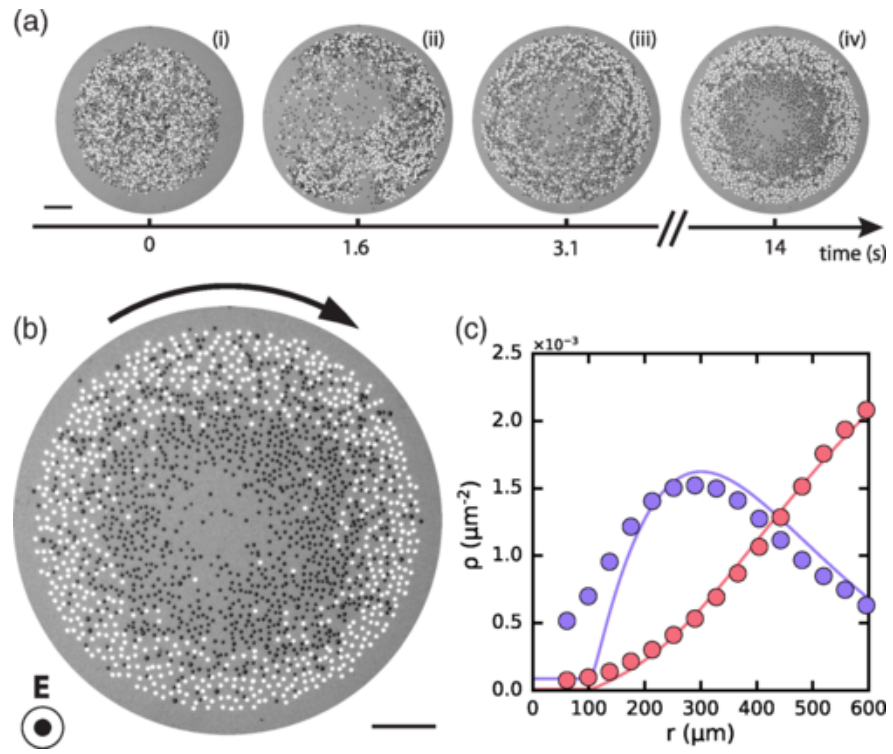


Figure 1.8: (a) The demixing process. (b) Steady state of binary colloidal flocks. (c) Radial density profiles of the two species. Adapted from [maity\\_spontaneous\\_2023](#)

different radii. In the simulation, the steric interaction with the wall was modeled as a Weeks-Chandler-Andersen potential and a torque reorienting the particle near the wall was inserted too.

For different circular confinement radii, the radial probability density  $P(r)$  was extracted, resulting in a striking agreement between simulations and experiments, as shown in Figure 1.9.

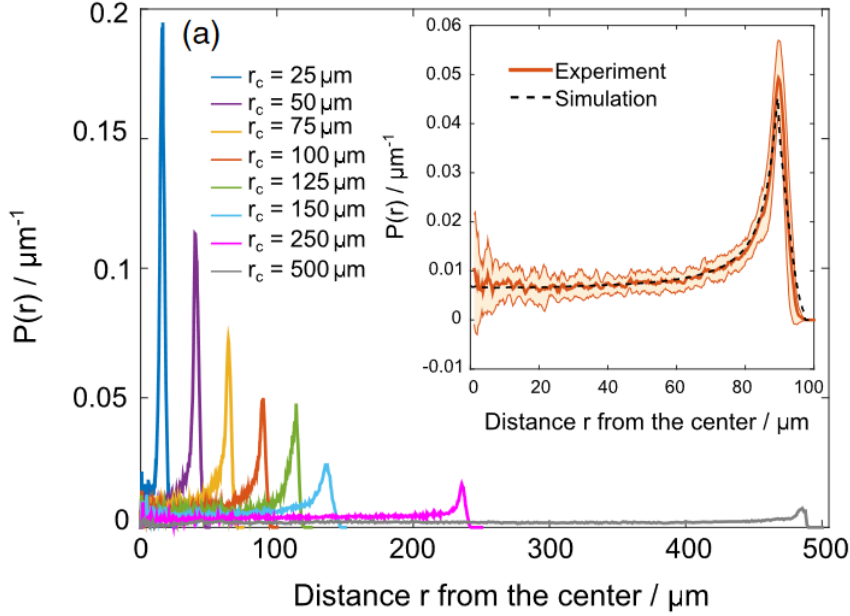


Figure 1.9: Experimental radial probability densities. Adapted from [ostapenko\\_curvature-guided\\_2018](#).

Next, [ostapenko\\_curvature-guided\\_2018](#) focus on how the swimming statistics depend on the radius of curvature. In order to do so, keeping the results independent from confinement size, simulations and experiments were performed within an elliptical chamber, with the result that the alga spent more time near the walls with the smaller curvature radius. The result is that near-wall swimming probability increases monotonically with the curvature (or decreases monotonically with the radius), and once again, there is a good agreement between experimental data and simulations.

### 1.3.3 Inference of interaction potentials

Inferring interaction potentials starting from experimental or simulated data is challenging and different techniques could be adopted. Since the real interactions that occur between a pair of colloidal particles are mostly unknown and in principle may involve chemical gradients, hydrodynamics, etc., it is essential to have a method that predicts forces between particles based on a central potential. Here, we will focus only on inference strategies based on Deep Learning (DL), which have shown particularly promising.

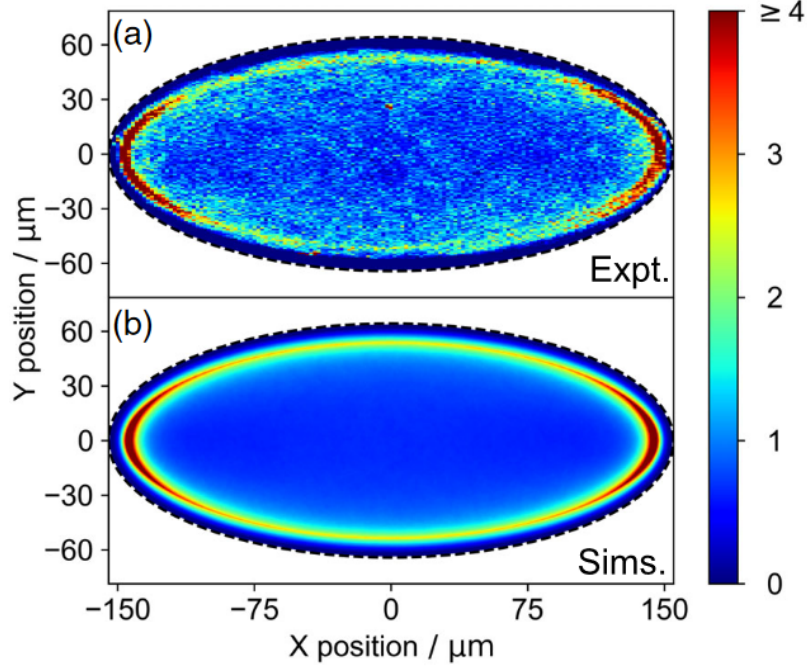


Figure 1.10: Comparison between relative probability density in (a) experiments and (b) simulations. Adapted from `ostapenko_curvature-guided_2018`.

In terms of machine learning model, the simplest approach is using some global attribute of the active particle ensemble to predict the potential via a Deep Neural Network (DNN). The idea is to concatenate all attributes in a vector and feed it as input to a DNN, that has as target function another vector containing the values of interaction potentials; the loss function to minimize is the difference (absolute or square) between the predicted potential and the ground-truth one. Ref. `bag_interaction_2021` aims at doing exactly that, exploiting a fact from statistical and matter physics; as authors claim, they use a theorem saying that “for the fluids with only pairwise interaction (quantum or classical), the pair potential  $V(r)$  that leads to a specific  $g(r)$  is unique” and the question of predicting which  $V(r)$  causes a specific structural correlation like  $g(r)$  or, equivalently,  $S(q)$  “is a well defined one”.

Authors simulated both passive and active Brownian particles to see the difference between equilibrium and non-equilibrium configurations. All the tested potential were of the form  $V(r_{ij}) = 4\varepsilon \left[ \left( \frac{\sigma}{r_{ij}} \right)^a - \lambda \left( \frac{\sigma}{r_{ij}} \right)^b \right]$  with different values of the parameters. Letting the system reach steady state and then taking 100 snapshots of the pair correlation function to train the network, the authors show a match between predicted and real potentials in all the possible phases: gas-like, crystal and liquid-like. (Figure 1.11)

The non-equilibrium case is a different matter: as soon as self-propulsion is involved, phenomena like MIPS start to occur, pushing the system to cluster. Some literature has introduced effective many-body attractive potential to explain the change in structure caused by particles’ motility, even in cases where just an ex-

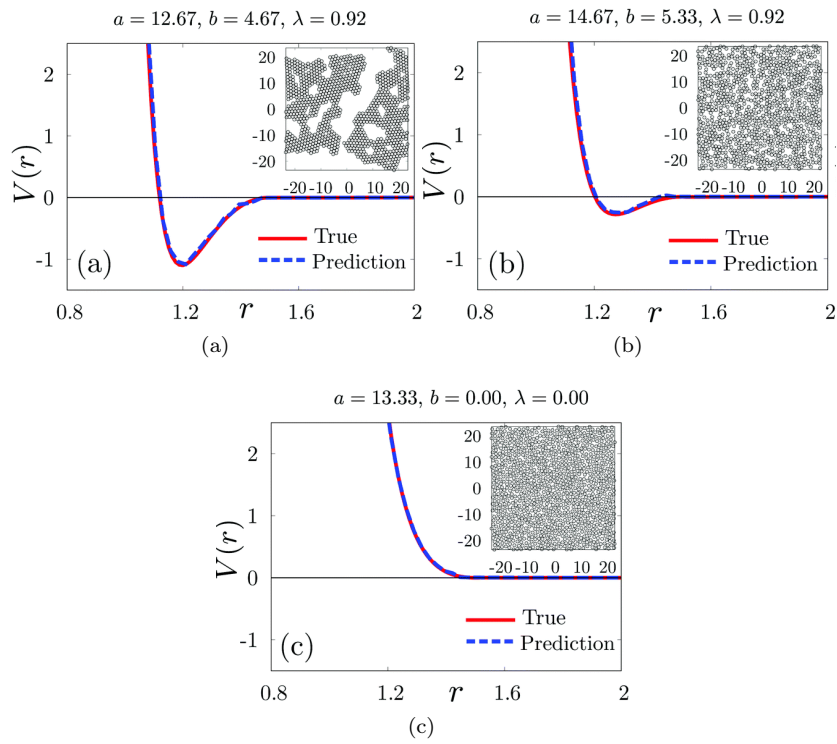


Figure 1.11: Potential shapes for different values of parameters `bag_interaction_2021`.



licit repulsion is present, and the results presented by **bag\_interaction\_2021** seem to point in that direction as well. As Figure 1.12(b) shows, pair correlation

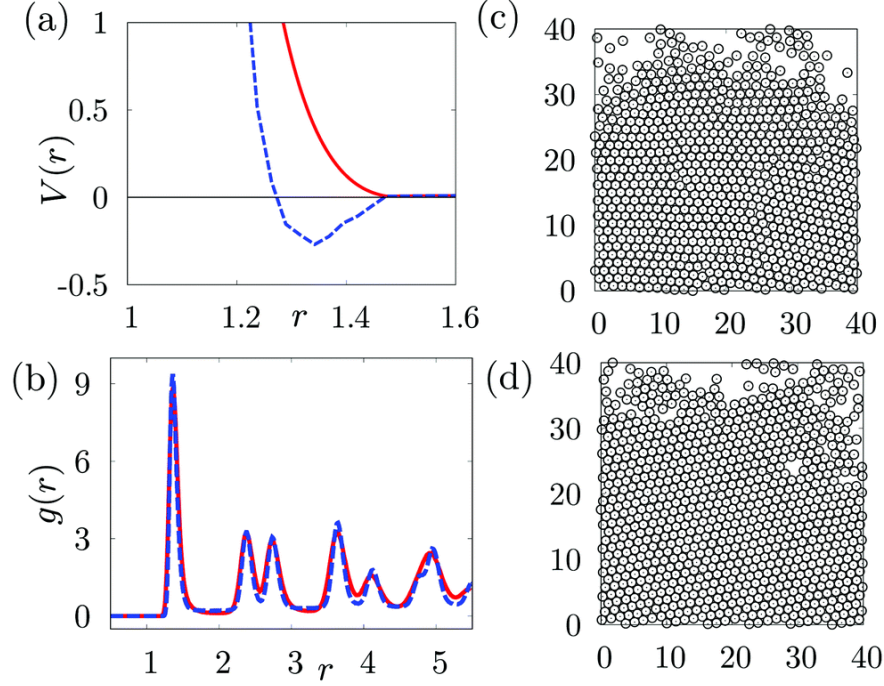


Figure 1.12: Equivalence between an equilibrium system with attraction and non-equilibrium one without attraction. Adapted from **bag\_interaction\_2021**.

functions in the case of active repulsive particles is similar to that of passive attractive particles, since only structure — i.e. particles' positions — is involved, tricking the network into predicting an attractive potential. This is a good result in a simulation context since it shows the capability of some methods to predict potentials starting from particle's positions and, though in out of equilibrium cases it does not work as desired, it sheds light on some theoretical statements. Nonetheless this approach does not fit the objective of the present thesis project, which tries to obtain actual 2-body interactions in active particle systems.

An alternative approach is working directly on positions and velocities of individual particles. It is an accepted fact that the best way to make AI learn something about a problem is having the invariances and symmetries of said problem taken in to account in the model design. The most efficient way to store information about a set of interacting bodies is a graph, where vertices represent single body information like position, velocity, mass or charge and edges contain information about the potential that make pairs of particles communicate. With these facts in mind, it is clear why Graph Neural Networks (GNNs or GNs) are so popular in several fields of physics. The distinction between GNNs and GNs is that the first one is a term that represent every kind on Neural Networks related with graphs, regardless the structure, while the Graph Network framework represents a specific network with a graph structure. An actual GN is actually a container, structured as a graph, which in principle holds three networks or functions, or models: one is the edge function  $\phi^e$ , which predicts edge features,



a node function  $\phi^v$  which predicts single nodes features and a global function  $\phi^u$  to predict global features.  $\phi^e$  maps from a pair of nodes and some information stored on the edge to a message vector which lies in the *latent space*. Then, all the messages from sending nodes into a receiving one are aggregated by means of a permutation-invariant function, namely sum, mean, max etc. The node model  $\phi^v$  takes the aggregated messages along with the node information and predicts some feature. Finally, a global function gathers all the information and predicts a global attribute **battaglia\_relational\_2018**.

In the case of interacting bodies, edge function works as the force law and node function plays the role of the second Newton’s law, calculating the resulting force and applying it to obtain particle’s acceleration. In **cranmer\_discovering\_2020** such an approach is applied to the case of Newtonian dynamics (along with Hamiltonian dynamics and a Dark Matter simulation, which we will not focus on) of a set of interacting particles. After simulating the dynamics of a set of interacting bodies with several kinds of interaction forces, **cranmer\_discovering\_2020** experiment with different message dimensionalities. Message dimensions is a topic that causes doubts when working with GNs and multiple strategies can be explored, the most natural of them is creating a bottleneck using the dimension of the problem, e.g. if particles move in N dimensions than forces are N-D and one may be tempted to think that, since messages should represent forces, this is the best dimensionality to use; the other approach is using a high-dimensional message, e.g. 100D, in training and then selecting the N most meaningful dimensions to plot the force in N-D. **cranmer\_discovering\_2020** try both of these strategies as well as a hybrid one: instead of implementing a hard bottleneck, they let the network learn with a 100D message but with regularization terms that encourage the model to learn compact representations of the forces, in accordance with an Occam’s razor type of reasoning. Doing this, the message is still 100-dimensional, but now most of its components have no variability, leaving few of them informational. Their results show that, although an explicit bottleneck works well, the best performing strategy is the  $L_1$  regularization. The whole workflow is explained in Figure 1.13.

Since all the operations that happen inside the node function are linear, it is evident that the message components will be some kind of linear combination of the actual forces. After letting the network train, one can search for the linear operation that minimizes the difference between the learned message components and the forces.

An alternative way of extracting the forces is using symbolic regression, which will give some insights about the functional form of the interaction potential. The modeling engine used is *eureqa*, and the best model is selected between several candidates at different complexity levels, choosing a more complicated one only when it is worth it.

The application to real active particles can make use some of these approaches, but it requires some tweaks with respect to the Newtonian dynamics approach. The most important change is in the physics: in a system without inertia, the meaning of acceleration is not clear and there is a linear relation between a force and a velocity. In this framework, **ruiz-garcia\_discovering\_2024** have developed a variant of the graph network by **cranmer\_discovering\_2020** that can work with active particles dynamics, called ActiveNet. In **ruiz-garcia\_discovering\_2024**, the graph network takes as input positions and orientations of a set of simulated active particles and tries to predict their velocity, given the instantaneous velocity

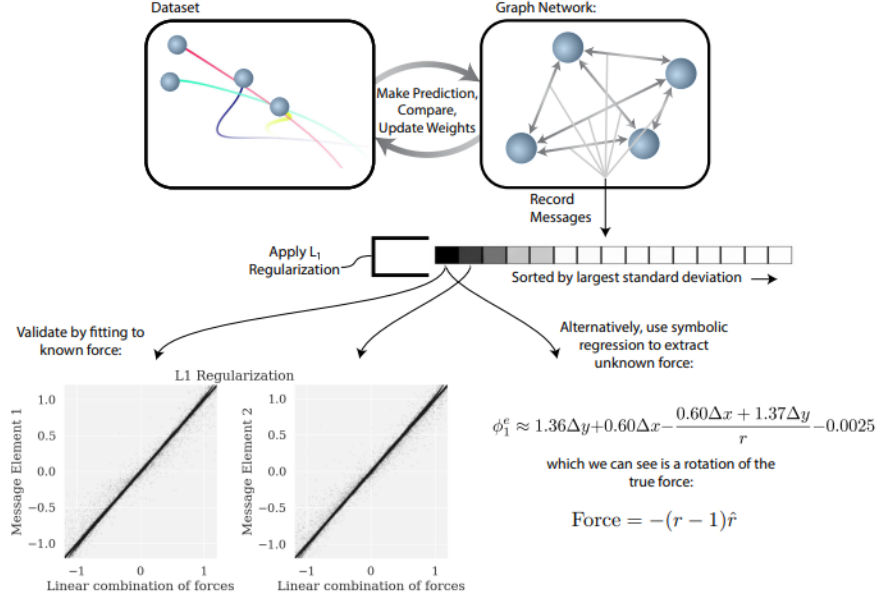


Figure 1.13: The GNN learning workflow in the case of Newtonian dynamics. Adapted from `cranmer_discovering_2020`.

$\frac{\vec{x}(t+\Delta t) - \vec{x}(t)}{\Delta t}$  as the ground truth. In this case the role of the node function is not only to predict the velocity starting from the sum of the forces, but also of learning and adding to it the self-propulsion velocity that drives the particles. This is a useful result, since after predicting the interaction force one can take the output of the node function and subtracting the edge function output in order to understand which part of the velocity can be explained through interaction and which is due to self-propulsion. A schematic representation of the ActiveNet GN is in Figure 1.14. In order to train the network, successive iterations are done, increasing the threshold distance to consider two particles as interacting. At the end of the training, the network gets tested and results show that it works well to predict both the self-propulsive force and the interaction potential. Having an internal way of taking into account the active velocity, this method works better than static structure-based ones, like `bag_interaction_2021`, in out of equilibrium particles ensembles where MIPS takes place, learning a repulsive interaction even though the system is clustered. Clearly, ActiveNet fails at short distance, since very few data are presented. Having Brownian motion at his base, the studied system has an internal degree of randomness. The goal of a machine learning task should be to reduce the loss (difference between ground truth and predictions) to make it as small as the noise. This can be useful to estimate the diffusion coefficient and works well even with few examples, as long as the temperature is high enough.

An important result of this paper is the application of the method to experimental data. The network needs some adjustments in order to work since experiments have some hurdles that must be overcome. To not be influenced by stuck particles, the network is fed with the bias that forces depend only on distances and not positions. Moreover, self-propulsion is forced to depend only

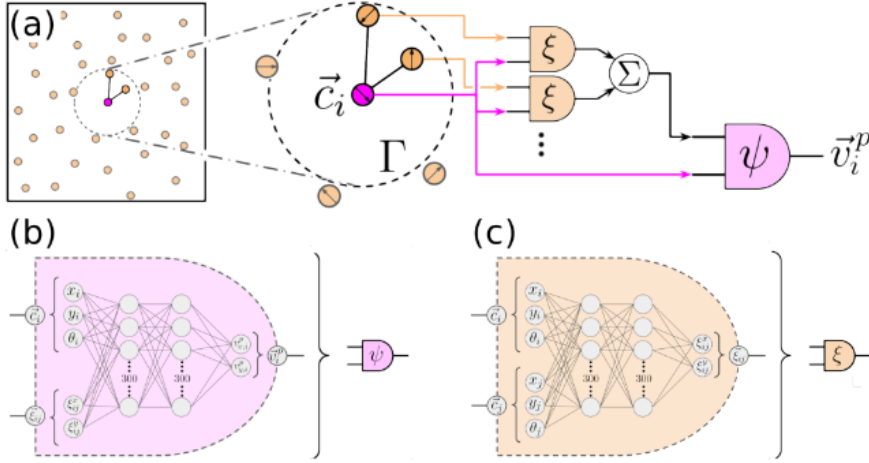


Figure 1.14: The ActiveNet structure. Adapted from [ruiz-garcia\\_discovering\\_2024](#).

on the orientation of particles. The experimental observations studied in that work contain thousands of particles with a clearly detectable in-plane orientation. Results show some similarities with the expectations but not much can be said since the actual interactions are not known exactly. Authors claim that probably symbolic regression is needed to discover the actual form of the interaction.

## 1.4 Background

### 1.4.1 Passive Brownian Motion

The first formulation of the theory of Brownian motion was obtained by Albert Einstein in a 1905 paper, where the mean square displacement was given in terms of a linear relation with time, with a diffusion coefficient  $D_t$  as  $\sqrt{\bar{x}^2} = \sqrt{2D_t t}$ . Here, we outline the derivation as it was presented by Paul Langevin some years afterwards, following [gardiner\\_handbook\\_2004](#).

It is known from statistical mechanics that a Brownian particle in equilibrium will have as mean kinetic energy

$$\langle \frac{1}{2}mv^2 \rangle = \frac{1}{2}k_B T \quad (1.6)$$

where  $T$  is the absolute temperature and  $k_B$  is Boltzmann's constant. If we assume the same formula as in macroscopic hydrodynamics, the viscous drag acting on the particle will be of the form  $-6\pi\eta a \frac{dx}{dt}$ , being  $a$  the particle's radius and  $\eta$  the viscosity of the fluid. Due to the random collisions with the fluid molecules, a passive Brownian particle experiences a *fluctuating force*  $X$ . The equation of motion for the particle is thus

$$m \frac{d^2x}{dt^2} = -6\pi\eta a \frac{dx}{dt} + X \quad (1.7)$$

which we multiply by  $x$  getting

$$\frac{m}{2} \frac{d^2}{dt^2} (x^2) - mv^2 = -3\pi\eta a \frac{d(x^2)}{dt} + Xx \quad (1.8)$$

where we called  $v = \frac{dx}{dt}$ . Averaging on the ensemble of particles we have

$$\frac{m}{2} \frac{d^2 \langle x^2 \rangle}{dt^2} + 3\pi\eta a \frac{d \langle x^2 \rangle}{dt} = k_B T \quad (1.9)$$

where the value for the mean kinetic energy was plugged in and we averaged the product  $Xx$  to zero, being  $X$  highly irregular (in modern times we just write everything in terms of a 0 mean Gaussian stochastic process, namely a Wiener process). The general solution to the differential equation for  $\langle x^2 \rangle$  is

$$\frac{d \langle x^2 \rangle}{dt} = \frac{k_B T}{3\pi\eta a} + C \exp(-6\pi\eta a t/m) \quad (1.10)$$

with  $C$  an arbitrary constant. It is possible to neglect the exponential, since Langevin estimated its characteristic time about  $10^{-8}$  s, and then integrate to get the equation

$$\langle x^2 \rangle - \langle x_0^2 \rangle = \frac{k_B T}{3\pi\eta a} t \quad (1.11)$$

which corresponds to what Einstein found out if  $D_t \equiv k_B T / (6\pi\eta a)$ .

Adapting this framework to our case-study, where the particle's orientation is considered, we need to take in to account both random forces and torques so that its motion is purely diffusive, both in position and orientation with the following diffusion coefficients

$$D_t = \frac{k_B T}{\gamma_t} \quad D_r = \frac{k_B T}{\gamma_r} \quad (1.12)$$

being  $\gamma_t = 6\pi\eta a$  and  $\gamma_r = 8\pi\eta a^3$  the respective drag coefficients, where  $a$  is the particle radius and  $\eta$  is the fluid viscosity. The basis to build the model upon is the Langevin equation

$$m\ddot{\mathbf{r}} = -\gamma_t \dot{\mathbf{r}} + \mathbf{F}_{th} \quad (1.13)$$

where  $\mathbf{F}_{th}$  is the random force given by the collisions with the fluid molecules.

Given that a typical Brownian particle will have a characteristic body-length in the order of  $\mu\text{m}$  and a velocity of  $\mu\text{m s}^{-1}$  the system can be studied in low-Reynolds number regime being

$$Re = \frac{\rho v a}{\eta} \sim 10^{-6} \quad (1.14)$$

where  $\rho$  is the fluid density,  $v$  is the particle speed,  $a$  is the particle radius and  $\eta$  is the fluid viscosity and the values of density and viscosity for water were plugged in. As a consequence of this fact, inertial effects can be neglected and it is possible to study the system in the *overdamped* regime, turning the Langevin equation 1.13 into

$$\gamma_t \dot{\mathbf{r}} = \mathbf{F}_{th} \quad (1.15)$$

which can be rewritten as:

$$\dot{\mathbf{r}} = \sqrt{2D_t} d\mathbf{W} \quad (1.16)$$

where  $d\mathbf{W}$  is the derivative of a zero-mean, unitary-variance Wiener process. In a homogeneous environment, rotational and translational motions are independent from each other, so that the equations of motion for a passive Brownian particle are

$$\dot{x} = \sqrt{2D_t} dW_x, \quad \dot{y} = \sqrt{2D_t} dW_y, \quad \dot{\theta} = \sqrt{2D_r} dW_\theta \quad (1.17)$$

### 1.4.2 Numerical Simulations of active particles

Despite the variety in single agent properties and self-propulsion mechanisms, it is possible to identify some key features that are shared between all active particle systems. The most important characteristic of an active, self-propelled particle is that, notwithstanding a symmetric shape (often in literature, and always in this work, spherical), each particle has a preferred axis which lies along the direction of self-propulsion.

With this hypothesis, rotational diffusion has now become relevant since the direction of self-propulsion varies randomly with a characteristic time scale which corresponds to the inverse of the rotational diffusion coefficient  $\tau_r = D_r^{-1}$ .

A simple and effective model to describe the dynamics of active particles is the Active Brownian Particle (ABP) model, which is a generalization of the Brownian particle model. This consists in adding a constant-magnitude self-propulsion velocity  $\mathbf{v}$  term to the equations of Brownian motion:

$$\dot{x} = v \cos \theta + \sqrt{2D_t} dW_x, \quad \dot{y} = v \sin \theta + \sqrt{2D_t} dW_y, \quad \dot{\theta} = \sqrt{2D_r} dW_\theta \quad (1.18)$$

where  $\theta$  is the particle orientation and  $v$  is the magnitude of the self-propulsion velocity.

As a consequence, the resulting finite-differences equations are:

$$\begin{cases} x_{n+1} = x_n + v \cos(\theta) \Delta t + \sqrt{2D_t \Delta t} W_{x,n}, \\ y_{n+1} = y_n + v \sin(\theta) \Delta t + \sqrt{2D_t \Delta t} W_{y,n}, \\ \theta_{n+1} = \theta_n + \omega \Delta t + \sqrt{2D_r \Delta t} W_{\theta,n} \end{cases} \quad (1.19)$$

where the case of a deterministic self-propulsion angular velocity  $\omega$  is also taken into account.

It is possible to insert external forces and torques in the system, where *external* means they are not due to the self-propulsion. Even though in literature there are examples of uniform external potentials, e.g. electric and magnetic fields, being applied on the ABP ensemble as a whole, in this work the only external force is the interaction between particles, which is applied in the low-Reynolds number regime as:

$$\begin{cases} x_{n+1} = x_n + \left( v \cos(\theta) + \frac{D_t}{k_B T} F_{ext,x} \right) \Delta t + \sqrt{2D_t \Delta t} W_{x,n}, \\ y_{n+1} = y_n + \left( v \sin(\theta) + \frac{D_t}{k_B T} F_{ext,y} \right) \Delta t + \sqrt{2D_t \Delta t} W_{y,n}, \\ \theta_{n+1} = \theta_n + \left( \omega + \frac{D_r}{k_B T} T_{ext} \right) \Delta t + \sqrt{2D_r \Delta t} W_{\theta,n} \end{cases} \quad (1.20)$$

where applying a force or a torque just linearly translates to a linear or angular velocity change, with the respective drag coefficients as proportionality constant.

### 1.4.3 Stochastic integration

The topic of integrating a stochastic differential equation (SDE) is a fundamental part of present work and an important object of investigation in the physics and mathematics community. The most simple SDE one can write is

$$\frac{dx}{dt} = f(x) + g(x)\xi(t) \quad (1.21)$$

in which  $\xi(t)$  is a stochastic process we assumed to be Gaussian with zero mean and no correlation at different times, which reads  $\langle \xi(t)\xi(t') \rangle = \delta(t - t')$ . If we define  $dW = \xi(t) dt$ , equation 1.21 is equivalent to

$$dx = f(x) dt + g(x) dW \quad (1.22)$$

where  $dW$  is the increment of a Wiener process  $W(t)$ , defined by its probability

$$P(W(t)) = \frac{1}{\sqrt{2\pi t}} e^{-\frac{W(t)^2}{2t}}. \quad (1.23)$$

Now, to solve such SDE, we need to compute integrals of the form  $\int W dW$ . We start by defining the mean square limit as

$$\text{m.s.} \lim_{n \rightarrow \infty} X_n = X \iff \lim_{n \rightarrow \infty} \langle (X_n - X)^2 \rangle = 0 \quad (1.24)$$

where the average  $\langle \cdot \rangle$  is taken over different realizations of the stochastic process. With this, the stochastic integral is defined in terms of a discrete sum

$$\int_0^t W dW = \text{m.s.} \lim_{n \rightarrow \infty} \sum_{i=1}^n W(t_i^*) [W(t_i) - W(t_{i-1})] \quad (1.25)$$

with  $t_{i-1} < t_i^* < t_i$ , that is better defined in terms of a constant  $\alpha$  as  $t_{i-1} + \alpha(t_i - t_{i-1})$ . Using the increment independence property of the Wiener process, we can compute the sum getting

$$\sum t_i - 1 + \alpha(t_i - t_{i-1}) = \alpha t \quad (1.26)$$

so that the result of the integral depends on  $\alpha$ . In principle, no value in  $[0, 1]$  is denied, but in literature only two values are found:  $\alpha = 0$ , which defines Itô method, and  $\alpha = 1/2$ , specific for Stratonovich method, which gives the *standard* result that can be obtained through Riemann integration.

With all of this, we are ready to integrate our SDE, formally

$$x(t) - x(0) = \int_0^t f(x(s)) ds + \int_0^t g(x(s)) dW \quad (1.27)$$

considering only the second term in the right-hand side, and Taylor-expanding it we get

$$\int_0^t g(x) dW \approx \int_0^t dW [g(x(0)) + g'(x(0))(x(s) - x(0))]. \quad (1.28)$$

The Itô versus Stratonovich controversy poses a subtle but fundamental problem: since  $g$  depends on  $x$  which depends on  $t$ , to compute the  $i$ -th step

when we have the  $i - 1$ -th we need to evaluate  $g$  at an instant  $t_i^*$ , subsequent to  $t_i$ , where the value of  $x$  is not known yet, in principle. Only the Itô prescription solves this issue, using the concept of *nonanticipating* functions.

With all of this said, it is possible to state that the type of calculus used, i.e. the value of  $\alpha$ , is actually a parameter of the model and there is literature showing that the physical quantities obtained through simulations are different if one chooses a method over another **mannella\_ito\_2012**.

Let us apply this theoretical notions to the equations for ABPs. One must be very careful when dealing with discretization step in stochastic integration, especially when dealing with nonlinear functions of noise terms, for it is difficult to know *a priori* which are the correct expansions at any order. Only accounting for  $\theta$  and  $x$ , we have

$$\begin{cases} dx = f_x(x) dt + v_0 \cos(\theta) dt + \sqrt{2D_t} dW_x \\ d\theta = \sqrt{2D_r} dW_\theta \end{cases} \quad (1.29)$$

where in  $f$  we included all possible interactions a particle can undergo. For now we set that part to 0 since it does not raise integration problems and consider only the terms which contain stochastic parts. We integrate to get

$$\begin{cases} x(h) - x(0) = \int_0^h v_0 \cos(\theta(s)) ds + \int_0^h \sqrt{2D_t} dW \\ \theta(s) - \theta(0) = \sqrt{2D_r s} \sim \mathcal{O}(\sqrt{s}) \end{cases} \quad (1.30)$$

being  $\int_0^s dW = \sqrt{s}Y_1$  with  $Y_1 \sim \mathcal{N}(0, 1)$ . We plug what obtained for  $\theta$  in the first order Taylor expansion of cosine to get ( $\theta_x \equiv \theta(x)$  for short)

$$x(h) - x(0) = \int_0^h v_0 [\cos(\theta_0) - \sin(\theta_0)(\theta_s - \theta_0)] ds + \int_0^h \sqrt{2D_t} dW \quad (1.31)$$

$$= \sqrt{2D_t h} Z_1 + h v_0 \cos \theta_0 - \sin \theta_0 Y_1 \sqrt{h} \int_0^h ds \quad (1.32)$$

with  $Z_1 \sim \mathcal{N}(0, 1)$ , and we notice that the last term is  $\mathcal{O}(h^{3/2})$ , leaving us with the first order unchanged. Having the right first order is fundamental because that is the order that enters in finite difference equations. We can thus conclude that finite difference equations in the form we wrote them in expressions 1.19-1.20 are the correct ones for our problem.

#### 1.4.4 Algorithms

A variety of algorithms to integrate SDEs have been reported in the literature. Here we only give the details of what has been used in present thesis.

The simplest method to integrate differential equation is the Euler scheme, which was first applied to ODEs in XVIII century. It is a first order method and it is the basis to all higher order schemes. As we did before, we take the first order expansion in the integration step  $h$  to integrate equation 1.22

$$x(h) - x(0) = \int_0^h (f_0 + g_0 \xi(t)) dt = h f_0 + g_0 \int_0^h \xi(t) dt \quad (1.33)$$

which in general is not correct: in stochastic integration, being  $\int_0^h dW \sim \mathcal{O}(\sqrt{h})$ , some unexpected  $\mathcal{O}(h)$  terms, which are combination of lower orders, tend to

appear. In particular, it is straightforward to show that the correct first order in  $h$  is

$$x(h) - x(0) = g_0 Z_1(h) + f_0 h + \frac{1}{2} g_0' g_0 Z_1(h)^2 \quad (1.34)$$

being  $Z_1 \sim \mathcal{N}(0, \sqrt{h})$  **mannella\_integration\_2011**.

Anyway, for cases like ours where noise is purely additive (i.e.  $g(x) = \sqrt{2D}$ ), the last term is 0 and the simple-minded first order is correct. Basically, this algorithm means that at any step one should propagate with the first order of the deterministic part and then add a randomly generated Gaussian number with 0 mean and the right variance. A pseudo code for Euler algorithm applied to the case of interacting ABPs is in Algorithm 1.

---

**Algorithm 1** The Euler algorithm

---

```

1: for n in timesteps do
2:   for i in particles in ensemble do
3:      $\vec{F}_{i,n} = \sum_j^{N_p} \vec{F}_{ij,n}$ 
4:      $w_{i,n} \sim \mathcal{N}(0, \sqrt{2D_t \Delta t})$ 
5:      $z_{i,n} \sim \mathcal{N}(0, \sqrt{2D_r \Delta t})$ 
6:      $\vec{r}_{i,n+1} \leftarrow \vec{r}_n + w_{i,n} + v(\cos \theta_{i,n}, \sin \theta_{i,n}) \Delta t + \vec{F}_{i,n} \Delta t / \gamma_t$ 
7:      $\theta_{i,n+1} \leftarrow \theta_{i,n} + z_{i,n} + \omega_{i,n} \Delta t + T_{i,n} \Delta t / \gamma_r$ 

```

---

The first higher order correction to Euler is the Heun scheme. This algorithm involves the calculation of an intermediate step  $x_{\text{int}}$  which helps in dealing with the nonlinearity of the deterministic function  $f$ . It works as follows

$$\begin{aligned} x_{\text{int}} &= x(0) + \sqrt{2D} Z_1(h) + f_0 h \\ x(h) &= x(0) + \sqrt{2D} Z_1(h) + \frac{h}{2} (f_0 + f(x_{\text{int}})). \end{aligned} \quad (1.35)$$

---

**Algorithm 2** The Heun algorithm

---

```

1: for n in timesteps do
2:   for i in particles in ensemble do
3:      $w_{i,n} \sim \mathcal{N}(0, \sqrt{2D_t \Delta t})$ 
4:      $z_{i,n} \sim \mathcal{N}(0, \sqrt{2D_r \Delta t})$ 
5:      $\vec{F}_{i,n} = \sum_j^{N_p} \vec{F}_{ij}(\vec{r}_{i,j}(\vec{r}_{i,n}, \vec{r}_{j,n}))$ 
6:      $\vec{r}_{i,\hat{n}} \leftarrow \vec{r}_n + w_{i,n} + v(\cos \theta_{i,n}, \sin \theta_{i,n}) \Delta t + \vec{F}_{i,n} \Delta t / \gamma_t$ 
7:      $\theta_{i,\hat{n}} \leftarrow \theta_{i,n} + z_{i,n} + \omega_{i,n} \Delta t + T_{i,n} \Delta t / \gamma_r$ 
8:      $\vec{F}_{i,\hat{n}} = \sum_j^{N_p} \vec{F}_{ij}(\vec{r}_{i,j}(\vec{r}_{i,\hat{n}}, \vec{r}_{j,\hat{n}}))$ 
9:      $\delta \vec{r} \leftarrow \frac{\Delta t}{2} \left[ v(\cos \theta_{i,n}, \sin \theta_{i,n}) + \vec{F}_{i,n} / \gamma_t + v(\cos \theta_{i,\hat{n}}, \sin \theta_{i,\hat{n}}) + \vec{F}_{i,\hat{n}} / \gamma_t \right]$ 
10:     $\vec{r}_{i,n+1} \leftarrow \vec{r}_n + w_{i,n} + \delta \vec{r}$ 
11:     $\theta_{i,n+1} \leftarrow \theta_{i,n} + z_{i,n} + \frac{\Delta t}{2} [\omega_{i,n} \Delta t + T_{i,n} / \gamma_r + \omega_{i,\hat{n}} \Delta t + T_{i,\hat{n}} / \gamma_r]$ 

```

---

Now one can ask which is the "best" algorithm. The answer lies in two distinct topics: deterministic accuracy and stochastic behavior. Regarding deterministic accuracy, one can analyze which is the order of the numerical error made in the integration, obtaining that, being a first order algorithm, Euler scheme is



accurate up to  $\mathcal{O}(h)$ , while Heun is  $\mathcal{O}(h^2)$ , making the latter preferable especially when working with highly nonlinear and steep potentials.

In order to analyze stochastic behavior, if one is interested in large time behavior, it is possible to study the equilibrium distribution  $P(x)$ . In particular, a system described by  $\dot{x} = -V'(x) + \sqrt{2D}\xi(t)$ , the equilibrium distribution should be  $P(x, \infty)_{\text{true}} = N \exp(-V(x)/D)$ , while a simulated distribution will be  $P(x, \infty)_{\text{true}} = N' \exp(-(V(x) + hS(h, x))/D)$ , with an error  $S$ . It is possible to show **mannella integration 2011** that for Euler  $S(h, x) = (V')^2/4 - DV''/2$  while Heun has  $\bar{S}(h, x) = \mathcal{O}(h)$ . For Heun error does not depend on the value of potential and its derivatives but only on integration step, making it possible to get more accurate estimates of the equilibrium distribution.

Analyses suggest that Heun scheme is among the most convenient algorithms, since higher order schemes do not do better, but they are much more expensive to implement on a computer.

Nonetheless, with respect to Euler, Heun is already more computationally expensive: if we restrict to the specific case of sets of interacting particles, the pseudo code in Algorithm 2 shows how this algorithm has to compute all the forces twice to perform a single step. However, in most cases the Heun scheme allows for large increases in simulation time steps compared to the Euler one, compensating for its higher single-step computational time and even making it possible to simulate larger times.